

# Extreme Graphical Models with Applications to Functional Neuronal Connectivity

*Andersen Chang*

*Department of Statistics, Rice University*

*Genevera I. Allen*

*Department of Electrical and Computer Engineering, Rice University,*

*Department of Computer Science, Rice University,*

*Department of Statistics, Rice University,*

*Department of Pediatrics-Neurology, Baylor College of Medicine,*

*Jan and Dan Duncan Neurological Research Institute, Texas Children's Hospital*

## **Abstract**

With modern calcium imaging technology, the activities of thousands of neurons can be recorded simultaneously *in vivo*. These experiments can potentially provide new insights into functional connectivity, defined as the statistical relationships between the spiking activity of neurons in the brain. As a commonly used tool for estimating conditional dependencies in high-dimensional settings, graphical models are a natural choice for analyzing calcium imaging data. However, raw neuronal activity recording data presents a unique challenge: the important information lies in the rare extreme value observations that indicate neuronal firing, as opposed to the non-extreme observations associated with inactivity. To address this issue, we develop a novel class of graphical models, called the extreme graphical model, which focuses on finding relationships between features with respect to the extreme values. Our model assumes the conditional distributions a subclass of the generalized normal or Subbotin distribution, and yields a form of a curved exponential family graphical model. We first derive the form of the joint multivariate distribution of the extreme graphical model and show the conditions under which it is normalizable. We then demonstrate the model selection consistency of our estimation method. Lastly, we study the empirical performance of the extreme graphical model through several simulation studies as well as through a real data example, in which we apply our method to a real-world calcium imaging data set.

**Keywords:** Calcium imaging; Exponential family graphical models; Extreme values; Generalized normal distribution; Graphical models; Subbotin distribution

## 1 Introduction

Undirected graphical models are a commonly used unsupervised learning tool for exploring and analyzing network structures and conditional relationships in multivariate data, especially in high-dimensional settings. These models have been used in a wide variety of applications, ranging from genomics (Allen and Liu, 2013) and network biology (Wang et. al., 2016) to finance and manufacturing (Talih and Hengartner, 2005), in order to answer various different research problems. Currently, there exists a broad literature on graphical models on the theoretical properties and estimation procedures for the Gaussian as well as other exponential family distribution models (Lauritzen, 1996; Yang et. al., 2015). In many of these expositions, it is typically inherently assumed that the observations in the data set are of equal importance when estimating a graph for the features in the data. In some contexts and research questions, however, this will not be the case. One particular example of unequal importance of observations occurs in the problem of extreme value modeling, where the main goal is to find significant relationships between variables with respect to rare extreme value observations rather than the average observations; common applications where this is relevant include risk quantification and management in finance (Rocco, 2014) and extreme weather event prediction in climatology (Buishead, 1989). With this type of problem, the ordinary graphical model distributions will not be useful for finding a scientifically meaningful graphical model estimate, as they have are designed to fit to the mean of all observations and not specifically to the extreme values.

One particular area of interest where graphical models are applied for problems of this type is the field of neuroscience, where they are used as a tool to help researchers analyze connections between individual neuronal activities in the brain. These interactions are often viewed in the framework of functional neuronal connectivity, defined as the statistical relationships between the activity of neurons in the brain (Biswal et. al., 1996). Graphical models are a natural choice for studying functional connectivity in calcium imaging data (Yatsenko et. al., 2015), which with modern technology can contain simultaneous *in vivo* recordings of thousands of neurons at a time. With this type of data, the most critical information lies in the times when each neuron is most active in terms of firing activity; these are indicated in the data by large positive spikes in the respective fluorescence traces. On the other hand, the non-extreme value observations are much more numerous

but are generally much less valuable, as they are mainly comprised of noise. Thus, in order to obtain scientifically meaningful functional connectivity estimates from calcium imaging data using graphical models, one must account for the fact that the important information that we want to model or predict is in the rare extreme values.

In the neuroscience literature, this issue is typically resolved using data preprocessing methods. Using this type of procedure, the raw fluorescence traces collected from a two-photon calcium imaging experiment are denoised and deconvolved to separate the positive extreme value spikes that indicate neuron firing activity from the smaller random fluctuations produced by measurement noise (Pnevmatikakis et. al., 2016). These methods commonly include applying an automatic thresholding procedure to zero out non-extreme value observations, theoretically leaving just the spikes in the fluorescence traces that would arise from neuronal activity. Gaussian graphical model methods are then applied to the deconvolved trace data in order to derive functional neuronal connectivity estimates (Rossant et. al., 2016; Chang, Yao, and Allen, 2019). While this type of approach is commonly used to analyze functional neuronal connectivity, it suffers from some potential drawbacks. Thresholding inherently causes some loss of data by setting all values which considered by the procedure to non-extreme to zero. However, for many data sets, such as calcium imaging data, the delineation between extreme and non-extreme values in the observations is not necessarily clear. Thus, thresholding can zero out an extreme value observation which contains important information or leave observations which are ultimately noise. Also, because the data analysis procedure described here is a multi-step pipeline, errors that arise from the data preprocessing step will propagate to the subsequent graph estimates, making them empirically less accurate than the theoretical convergence rate.

One potential alternative solution to the problem of model selection for extreme values from the current graphical model literature is the quantile graphical model (Ali, Kolter, and Tibshriani, 2016), specifically used at a very high or very low quantile in order to fit to the extreme values. This potentially removes the need to pre-process the data, as the quantile graphical model will increase the relative importance of extreme values in a data set compared to a Gaussian graphical model if an appropriate quantile is chosen, without needing to threshold the data as described previously. However, quantile graphical models have several issues as well that can arise when applied in these types of situations. The results from the quantile graphical model will depend substantially on the chosen quantile, as the choice of quantile can heavily impact the resulting objective function and how each observation is weighted. Adding to this, the selection of the appropriate quantile to use for a particular data set can be extremely difficult, as it is not perfectly clear how to select a specific quantile to use when the number and magnitude of the extreme values can vary substantially between the each of the variables in a data set. Another potential downside to the quantile graphical model is that it weighs the

extreme positive and extreme negative values asymmetrically, only increasing the weight of one side while decreasing the weight of the other. Therefore, this type of model may not be useful in contexts where a single data set could have both.

In this paper, we introduce a new class of probabilistic graphical model called the extreme graphical model which can be used to find conditional dependencies between variables based on extreme value observations. The basis of the graphical model is the generalized normal distribution, also known as the Subbotin distribution (Nadarajah, 2005). With any power greater than 2, the generalized normal distribution will have thinner tails when compared to a Gaussian distribution, which in turn comparatively increases the weight of large differences between an observation and its estimated expected value in the corresponding likelihood function. This means that parameter estimates from a generalized normal distribution with power greater than 2 will be more heavily weighted towards the observed extreme values of a data set, relative to parameter estimates from a Gaussian distribution. Thus, we propose to use a construction of a multivariate generalized normal distribution with a power greater than 2 as a graphical model distribution for analyzing data sets where the goal is to find relationships between variables based on their extreme value observations. While different definitions of a multivariate generalized normal distribution have been proposed and explored before (Goodman and Kotz, 1973; Verdoolege and Scheunders, 2012), ours is the first to be defined as a valid graphical model distribution, with easily interpretable conditional independence conditions. Compared to models currently used in the literature for this type of problem, the extreme graphical model has several advantages; it does not require the usage of data pre-processing methods in order to find statistical relationships with respect to the extreme values, and it smoothly increases the relative importance of extreme value observations by their magnitude.

The rest of this paper is structured as follows. In section 2, we introduce the extreme graphical model by defining its node-wise conditional distribution, and derive the joint multivariate distribution of the graphical model using results from the Hammersley-Clifford theorem. In section 3, we introduce the estimation algorithm and explore its theoretical properties. In section 4, we investigate the performance of the extreme graphical model on simulation studies and compare it to state-of-the-art methods. Finally, in section 5, we apply our method to a real-world calcium imaging data set to estimate a functional neuronal connectivity graph and explore the results.

## 2 Extreme Graphical Model

Suppose we have a random data matrix  $\mathbf{X} \in \mathbb{R}^{n \times p}$  for which we would like to estimate pairwise conditional relationships between the features, specifically with respect to the observed extreme values. In this particular context, we presume that the extreme value events are empirically rare relative to the number of total

observations, and therefore in order to see extreme events in the data we need the number of observations  $n$  to be large relative to the number of variables  $p$ . To create a class of graphical model appropriate for analyzing this type of data, we follow the methodology utilized in (Besag, 1974) and (Yang et. al., 2012). In these papers, the form of the graphical model distribution is established by first defining the node-wise conditional distributions, and then using them to construct the joint multivariate distribution. For the extreme graphical model, we propose to use the generalized normal distribution as the node-wise conditional distribution for each individual feature. The univariate generalized normal distribution with location parameter  $\mu$ , scale parameter  $\sigma$ , and shape parameter  $\nu$  takes the functional form

$$f(x) = \frac{1}{2\sigma\Gamma\left(\frac{1+\nu}{\nu}\right)} e^{-\left(\frac{|x-\mu|}{\sigma}\right)^\nu}, \quad x \in \mathbb{R}. \quad (1)$$

Here, we assume that  $\nu$  is known or selected a priori rather than estimated. If  $\nu = 2$ , then generalized normal distribution is proportionally equivalent to the Gaussian distribution. For any  $\nu > 2$ , the generalized normal distribution will have thinner tails relative to the Gaussian, i.e. any large magnitude values of  $x$  will have a lower probability density relative to the Gaussian. Therefore, in this setting, any extreme value observations of  $x$  will have a much larger impact on any parameter estimates, since the generalized normal model with  $\nu > 2$  assumes that these extreme values are much less likely to occur when compared to the Gaussian case.

Because of the aforementioned properties, we choose to use the generalized normal with  $\nu > 2$  as the node-wise conditional distribution for the extreme graphical model. Throughout the rest of this paper, for simplicity of notation, we let  $\mu = 0$  and  $\sigma = 1$ . We will also strictly study the case where  $\nu$  is an even integer greater than 2. With these particular parameter values set, we can cast Equation 1 as a node-wise conditional distribution of the form

$$f(x_i|\mathbf{x}_{-i}) = \frac{1}{2\Gamma\left(\frac{1+\nu}{\nu}\right)} e^{-\left(\theta_{ii}x_i - \left(\sum_{j \neq i} \theta_{ij}x_j\right)\right)^\nu}, \quad x_i \in \mathbb{R}, \quad \nu > 2. \quad (2)$$

Here, the conditional relationships between a pair of variables  $x_i$  and  $x_j$  are assumed to be linear in nature and are represented by the parameter  $\theta_{ij}$ . If the parameter  $\theta_{ij}$  is zero, then it is trivial to show that  $x_i$  and  $x_j$  are conditionally linearly independent given all of the other variables in  $\mathbf{X}$ . Just as for Equation 1, the estimates of the model parameters  $\theta_{ij}$  will be more heavily weighted towards fitting to the extreme value observations of  $x_i$  when  $\nu > 2$  relative to a Gaussian distribution.

For the cases which are applicable for the extreme graphical model distribution, i.e. when  $\nu > 2$ , the resulting node-wise conditional distribution is a special case of a curved exponential family distribution, as opposed to the more commonly used exponential family distribution. Because of this, our method is not conducive to straightforward applications of results from the exponential family graphical model literature. Also, as a whole, properties of probabilistic graphical model distributions

stemming from this type of node-wise conditional distribution have not been well-studied in the literature. Therefore, in order to formulate the joint graphical model distribution for the extreme graphical model, we utilize the most general method as originally postulated in (Besag, 1974). In that paper, the author shows how joint multivariate graphical model distributions can be constructed from any set of valid node-wise conditional distributions by applying the most general form of a valid graphical model distribution, as proven via the Hammersley-Clifford theorem (Hammersley and Clifford, 1971). Here, we apply these same ideas specifically for the generalized normal node-wise conditional distribution in Equation 2 in order to derive the joint graphical model distribution. The result is shown in the following theorem.

**Theorem 1** (Joint Distribution of the Multivariate Subbotin). *Suppose  $(x_1, x_2, \dots, x_p)$  is a  $p$ -dimensional random vector, and its node-wise conditional distributions are given by:*

$$f(x_i | \mathbf{x}_{-i}) = \frac{1}{2\Gamma(\frac{1+\nu}{\nu})} e^{-(\theta_{ii}x_i - \sum_{j \neq i} \theta_{ij}x_j)^\nu}, \quad x_i \in \mathbb{R}$$

*for some even integer  $\nu$ . Then the joint graphical model distribution is given by*

$$f(\mathbf{x}) = \exp \left( \sum_{i=1}^p \left( -(\theta_{ii}x_i - \sum_{j < i} \theta_{ij}x_j)^\nu + (\sum_{j < i} \theta_{ij}x_j)^\nu \right) - A(\boldsymbol{\Theta}) \right) \quad (3)$$

*where  $\boldsymbol{\Theta}$  is the parameter matrix, i.e. the collection of all model parameters  $\theta_{ij}$ .*

As follows from our premise for Equation 1, it is assumed for this distribution that  $\nu$  is not innately a parameter to be estimated through the neighborhood selection process, but rather a hyperparameter of the overall graphical model. In the case where  $\nu = 2$ , the distribution given by Equation 3 is proportional to the multivariate Gaussian distribution, which we formalize below in Corollary 1.

**Corollary 1** (Gaussian Equivalence). *Consider the extreme graphical model distribution from Equation 3. Let  $\nu = 2$ . Then the extreme graphical model distribution will be equivalent to the multivariate Gaussian distribution with inverse covariance matrix  $\boldsymbol{\Theta}$ .*

In general, for the extreme graphical model, the log normalizing constant for the joint distribution  $A(\boldsymbol{\Theta})$  does not have a closed form solution. However, using the estimation procedure described in section 3, we do not need to have a closed form solution for  $A(\boldsymbol{\Theta})$  in order to estimate the graph structure for the joint graphical model distribution, as long as we have a closed form for each of the node-wise conditional distributions. Also, while we do not know the analytical solution for  $A(\boldsymbol{\Theta})$ , we can still find the condition under which it will be finite and positive and thus when full graphical model distribution will exist; this result is stated in Theorem 2 below.

**Theorem 2** (Normalizing Condition). *Consider the extreme graphical model distribution from Equation 3. Define the matrix  $\Theta$  such that*

$$\Theta_{ij} = \begin{cases} \theta_{ii} & i = j \\ -\theta_{ij} & i \neq j \end{cases}.$$

*Then the distribution will be normalizable if and only if  $\Theta$  is positive definite.*

We note that the statement of Theorem 2 shows that the normalizing condition for the extreme graphical model distribution is the same as that for the multivariate Gaussian distribution, regardless of which value of  $\nu$  is chosen. A full proof of Theorems 1 and 2 can be found in the Appendix.

### 3 Extreme Graph Model Selection

To estimate the edge set of the graph, we apply the neighborhood selection approach for sparse graphical model selection (Meinshausen and Bühlmann, 2006; Ravikumar, Wainwright, and Lafferty, 2010). Here, instead of using a full likelihood of the joint graphical model distribution, we combine feature selection estimates for the node-wise conditional distributions in order to estimate the graph structure. For each individual node  $x_i$ , we can estimate its graph neighborhood, defined as the minimal set such that  $x_i$  is conditionally independent of all remaining variables, by applying a generalized linear regression model predicting  $x_i$  from all other variables in the data set. An  $\ell_1$  regularization penalty is added to the regression problem in order to induce sparsity in the selected number of relevant features. After estimating the individual neighborhoods, the node-wise parameter estimates can be fused together to create a single graph estimate by selecting as the edge set for the graph all pairs of nodes which have a non-zero linear relationship with one another in both directions, i.e. all cases where a node  $x_i$  is considered to be a neighbor of  $x_j$  and  $x_j$  is considered to be a neighbor of  $x_i$ . Alternatively, we can select as neighbors all pairs of nodes which have a non-zero linear relationship with one another in only one direction, i.e. cases where a node  $x_i$  is considered to be a neighbor of  $x_j$  or  $x_j$  is considered to be a neighbor of  $x_i$ , but not necessarily both. As has been shown in previous literature, these two schemes will be asymptotically equivalent (Meinshausen and Bühlmann, 2006). For the generalized normal distribution with power  $\nu$ , the corresponding generalized linear model is the  $\ell_\nu$ -norm linear regression model (Money et. al., 1982), i.e.

$$\hat{\theta}_{ij} = \arg \min_{\theta_{ij}} \frac{1}{\nu N} \|\mathbf{x}_i - \mathbf{X}_{-i} \theta_{ij}\|_\nu^\nu$$

where  $\mathbf{X}_{-i}$  denotes all columns of  $\mathbf{X}$  except for column  $i$ . Combining the above with the Lasso regularization penalty gives us the objective function

$$\hat{\theta}_{ij} = \arg \min_{\theta_{ij}} \frac{1}{\nu N} \|\mathbf{x}_i - \mathbf{X}_{-i} \theta_{ij}\|_\nu^\nu + \lambda \|\theta_{ij}\|_1.$$

This is equivalent to the Extreme Lasso regression model as defined by (Chang, Wang, and Allen, 2020), and the parameters for the regression problem can be estimated using the algorithmic procedure outlined in the aforementioned paper.

Below, we present the finite sample performance guarantees for the estimation procedure described, and we show that it is variable selection consistent. To do this, we utilize the performance guarantees for the Extreme Lasso in the feature selection problem, which have been studied previously in (Chang, Wang, and Allen, 2020). There, the authors show that the Extreme Lasso is variable selection consistent with a known convergence rate; the full statements and proofs can be in that paper. Using the results for the Extreme Lasso, we can derive the performance guarantees for the extreme graphical model. Formally, let us define the true edge set of the full graph as

$$E = \{(i, j) : \theta_{ij} \neq 0\}$$

and the true set of neighbors of each node  $i \in \{1, 2, \dots, p\}$  as

$$S_i = \{j \in \{1, 2, \dots, p\} \setminus i : (i, j) \in E\}.$$

We also denote the Fisher information matrix of the joint multivariate distribution as  $Q$  and the Fisher information sub-matrix for the true set of neighbors of each node as  $Q_{S_i S_i}$ . For the theorem below, we require the following conditions:

1. **Bounded eigenvalues:** For all  $i \in \{1, 2, 3, \dots, p\}$ , there exists some  $B_{min} > 0$  and  $B_{max} > 0$  such that

$$B_{max} > \Lambda_{\min}(Q_{S_i S_i}) > B_{min}.$$

2. **Incoherence:** There exists a constant  $\alpha > 0$  such that

$$\|Q_{S_i^c S_i} Q_{S_i S_i}^{-1}\|_\infty < 1 - \alpha.$$

3.  **$\theta$ -min:** Let

$$\min_{(i,j) \in E} |\theta_{ij}| > \left( \frac{\tau}{\kappa_{IC}} \cdot \frac{1}{4} + 1 \right) \cdot \frac{2\sqrt{s}}{\kappa_{\mathcal{L}}} \cdot \frac{4\kappa_{IC}}{\tau} \nu \sqrt{\frac{\log p}{n}} \left[ 2\sqrt{\frac{2}{\nu}} + \sqrt{\frac{\log p}{n}} \right].$$

With these, we can now state the model selection consistency results of our method.

**Theorem 3 (Graphical Model Selection Consistency).** *Consider the extreme graphical model distribution from Equation 3. Assume that Conditions 1 and 2 hold. Suppose the regularization parameters for the estimation procedure satisfy*

$$\lambda_n \geq \frac{4\kappa_{IC}}{\tau} \nu \sqrt{\frac{\log p}{n}} \left[ 2\sqrt{\frac{2}{\nu}} + \sqrt{\frac{\log p}{n}} \right]$$

where  $\kappa_{IC}$  is the compatibility constant defined in Lee (2015). Then, the following properties holds with probability greater than  $1 - c_1 \exp(-c_2 \log p)$ :

- (i) The estimated edge set has a unique solution with support contained within the true edge set, i.e.  $\hat{E} \subset E$ .
- (ii) Additionally, if Condition 3 holds, then  $\hat{E}$  is also sign consistent, i.e.  $\text{sign}(\hat{E}) = \text{sign}(E)$ .

The full proof of the statement of Theorem 2 can be found in the Appendix. From the result above, we can see that the estimation procedure is variable selection consistent with respect to estimation of the true network. We note that the concentration bound for the extreme graphical model is a substantially weaker bound compared to that for a Gaussian graphical model with a neighborhood selection approach; this means that the extreme graphical model will generally require a relatively larger number of samples in order to achieve the same level of accuracy. However, as mentioned previously, we expect that the number of observations  $n$  will be large relative to the number of variables  $p$  in the contexts where we would apply the extreme graphical model. Thus, the slower convergence rate should not have a substantial impact empirically on the reliability of the estimates from the extreme graphical model.

As part of the model selection process, values for the hyperparameters  $\nu$  and  $\lambda$ , which control the influence of extreme values and the sparsity level of graph, respectively, need to be chosen as well. A number of methods for graph hyperparameter selection have been studied in the literature; for the extreme graphical model, we propose to use a stability selection approach (Meinshausen and Bühlmann, 2010). With this method, we utilize a bootstrapping approach to find the probability that each possible edge in the graph will be selected in a graph estimate using random resampling of data for given values of  $\nu$  and  $\lambda$ . We can then calculate an overall stability metric of graph selection for each pairing of  $\nu$  and  $\lambda$  tested using the criterion outlined in (Liu, Roeder, and Wasserman, 2010), and select the one that gives the most stable graph estimate on average. We keep as the final graph estimate all edges with a selection probability above a pre-defined threshold.

## 4 Simulation Study

We now study the performance of the extreme graphical model on various simulations. We generate data from a variety of models with a known underlying network structure. We compare our extreme graphical model method to Gaussian neighborhood selection, the graphical Lasso, and the quantile graphical model. For each simulation set, we show the average and standard deviation of the true positive rates and false discovery proportions for each method with respect to estimating the true edge set of the underlying graph across 5 replications. Below, we analyze the performance when hyperparameter selection is performed for all methods using

approximate oracle sparsity tuning. We also show results for these simulation studies using data-driven stability selection hyperparameter tuning in the Appendix.

#### 4.1 Extreme Graphical Model Distribution

For our first set of simulations, we investigate the efficacy of our estimation procedure on the multivariate graphical model distribution from which it is derived. As a baseline simulation, we generate  $n = 2000$  observations and  $p = 100$  features from the extreme graphical model distribution as defined in Equation 3 with  $\nu = 8$ , using a Gibbs sampling procedure with the univariate node-wise conditional distributions as defined in Equation 2. The network parameter matrix  $\Theta$  is structured as a sparse small world graph with 5 total cliques. We compare the extreme graphical model for  $\nu = 4, 6$  and  $8$ , the Gaussian graphical model estimated using neighborhood selection and the graphical Lasso, and the quantile graphical model at the 50th and 90th percentiles. We then vary the number of observations and features, the  $\nu$  parameter of the extreme graphical model distribution, and the structure of the underlying graph and analyze how the performance of each method changes.

Table 1 show the results of the simulations. In general, the extreme neighborhood selection algorithm is able to identify the true network structure of the multivariate generalized normalized distribution with fairly high accuracy. We also see that the Gaussian graphical models and the median quantile graphical model performs relatively well in terms of model selection, while the quantile graphical model at the 90th percentile generally performs much worse. The former of these results are unsurprising; since the probability density function of the extreme graphical model distribution is still a symmetric bell-shaped curve around the location parameter, and because the overall empirical correlation structure of the generated distribution will still be very close true parameter matrix, we would expect the graphical models which fit toward the mean or the median to do well. On the other hand, sampling from the multivariate generalized normal distribution is unlikely to generate contemporaneous extreme values between two variables which are related in the parameter matrix, as it is a thin tailed distribution. Thus, the quantile graphical models with high quantiles are unlikely to estimate the true network structure well, which we see reflected in the results. Comparing the results for simulation parameters, we see that reducing the number of observations and increasing the number of features decreases the true positive rate for all methods, with a greater impact on the Gaussian graphical model in the former and the extreme graphical model in the latter. We also see that the extreme graphical model with the true  $\nu$  always has the best performance, which we would expect. Finally, we see that the extreme graphical model does best for all the various types of graph structures, although the true positive rate decreases more severely for non-small world graphs.

Tab. 1: Average TPR, FDP. (std. devs) for multivariate extreme graphical model distribution simulations with oracle tuning, averaged over 5 replicates. Best performing methods are boldfaced.

Model	Baseline			
	TPR	FDP		
Extreme (4)	0.793 (0.058)	0.205 (0.059)		
Extreme (6)	0.812 (0.054)	0.200 (0.050)		
Extreme (8)	<b>0.840</b> (0.052)	<b>0.166</b> (0.053)		
Gaussian Glasso	0.756 (0.053)	0.238 (0.054)		
Gaussian NS	0.779 (0.061)	0.215 (0.059)		
Quantile (0.5)	0.689 (0.075)	0.223 (0.079)		
Quantile (0.9)	0.277 (0.083)	0.727 (0.087)		
	<i>n</i> = 1000		<i>n</i> = 4000	
Model	TPR	FDP	TPR	FDP
	0.534 (0.058)	0.469 (0.059)	0.853 (0.052)	0.150 (0.054)
Extreme (6)	0.564 (0.062)	0.441 (0.060)	0.859 (0.051)	0.142 (0.053)
Extreme (8)	<b>0.631</b> (0.055)	<b>0.367</b> (0.053)	<b>0.893</b> (0.055)	<b>0.105</b> (0.055)
Gaussian Glasso	0.497 (0.055)	0.491 (0.054)	0.854 (0.051)	0.126 (0.054)
Gaussian NS	0.503 (0.059)	0.490 (0.059)	0.863 (0.048)	0.125 (0.047)
Quantile (0.5)	0.482 (0.079)	0.520 (0.075)	0.817 (0.071)	0.172 (0.073)
Quantile (0.9)	0.259 (0.081)	0.744 (0.084)	0.345 (0.077)	0.652 (0.075)
	<i>p</i> = 300		<i>p</i> = 1000	
Model	TPR	FDP	TPR	FDP
	0.684 (0.058)	0.311 (0.056)	0.503 (0.059)	0.501 (0.060)
Extreme (6)	0.732 (0.059)	0.272 (0.055)	<b>0.563</b> (0.053)	<b>0.438</b> (0.056)
Extreme (8)	<b>0.751</b> (0.056)	<b>0.250</b> (0.054)	0.545 (0.061)	0.452 (0.055)
Gaussian Glasso	0.616 (0.050)	0.388 (0.049)	0.480 (0.053)	0.518 (0.055)
Gaussian NS	0.634 (0.053)	0.362 (0.056)	0.471 (0.057)	0.507 (0.055)
Quantile (0.5)	0.573 (0.078)	0.427 (0.081)	0.416 (0.077)	0.590 (0.078)
Quantile (0.9)	0.265 (0.085)	0.747 (0.085)	0.284 (0.079)	0.731 (0.082)
	$\nu$ = 4		$\nu$ = 6	
Model	TPR	FDP	TPR	FDP
	<b>0.886</b> (0.053)	<b>0.107</b> (0.054)	0.823 (0.060)	0.170 (0.059)
Extreme (6)	0.842 (0.057)	0.158 (0.055)	<b>0.855</b> (0.057)	<b>0.137</b> (0.057)
Extreme (8)	0.734 (0.062)	0.261 (0.058)	0.775 (0.051)	0.218 (0.058)
Gaussian Glasso	0.872 (0.053)	0.122 (0.054)	0.827 (0.053)	0.171 (0.054)
Gaussian NS	0.865 (0.053)	0.134 (0.050)	0.779 (0.051)	0.225 (0.059)
Quantile (0.5)	0.664 (0.072)	0.335 (0.073)	0.626 (0.072)	0.381 (0.079)
Quantile (0.9)	0.252 (0.079)	0.776 (0.081)	0.250 (0.080)	0.746 (0.083)
	Chain		Erdos-Renyi	
Model	TPR	FDP	TPR	FDP
	0.696 (0.052)	0.304 (0.059)	0.644 (0.056)	0.358 (0.057)
Extreme (6)	0.711 (0.054)	0.290 (0.050)	0.659 (0.054)	0.346 (0.061)
Extreme (8)	<b>0.733</b> (0.058)	<b>0.271</b> (0.055)	<b>0.672</b> (0.061)	<b>0.329</b> (0.057)
Gaussian Glasso	0.653 (0.049)	0.348 (0.051)	0.615 (0.052)	0.238 (0.070)
Gaussian NS	0.667 (0.058)	0.335 (0.056)	0.629 (0.060)	0.374 (0.059)
Quantile (0.5)	0.569 (0.072)	0.338 (0.071)	0.556 (0.071)	0.452 (0.073)
Quantile (0.9)	0.225 (0.083)	0.786 (0.084)	0.234 (0.086)	0.768 (0.079)

## 4.2 Artificial Neuronal Network

We now investigate a simulation study which is based upon neuroscience applications. Here, we simulate data from the balanced network model of (Akil, Rosenbaum, and Josić, 2020), which utilizes a neuronal spiking model in order to create data which emulates the physical processes which comprise functional neuronal connectivity. In particular, the balanced network generates correlated spiking patterns between variables over time, mimicking the behavior of neurons as observed during calcium imaging experiments. The output of the balanced neuronal network algorithm is a set of spike times for each neuron, which we denote as the set

$$T = \{(i, j) \mid \text{neuron } j \text{ spikes at time } i\}.$$

To replicate fluorescence traces from calcium imaging, we then simulate each neuron's activity as an AR(1) process with innovations at the times specified by  $T$ :

$$\begin{aligned} X_{ij} &= \alpha \mathbf{X}_{i-1,j} + [\mathbb{1}_{\{(i, j)\}}(T)] Z_{ij} + \epsilon_{ij} \\ Z &\sim N(\mu, 1) \\ \epsilon &\sim N(0, 1). \end{aligned}$$

Here, we consider the true underlying graph to be comprised of edges which connect all pairs of simulated neurons which spike contemporaneously, i.e

$$G = \{(j, k) \mid \exists i : (i, j) \in T \cap (i, k) \in T\}.$$

For this simulation study, we use as a baseline case  $n = 5000$  time points for  $p = 100$  simulated neurons, along with parameter values  $\alpha = 0.5$  and  $\mu = 20$ . We also limit the spike rate of the variables such that spikes occur at a maximum of 0.001 Hz in order to emulate the rarity of the extreme values that are seen in real-world fluorescence trace data. We compare the extreme graphical model for  $\nu = 4, 6$  and  $8$ , the Gaussian graphical model estimated using neighborhood selection and the graphical Lasso, and the quantile graphical model at the 50th, 90th, 99th, and 99.9th percentiles. We also vary the number of simulated neurons, the maximum spiking rate, and the average size of each spike in the simulations below.

Tab. 2: Average TPR, FDP. (std. devs) for balanced neuronal network simulations with oracle tuning, averaged over 5 replicates. Best performing methods are boldfaced.

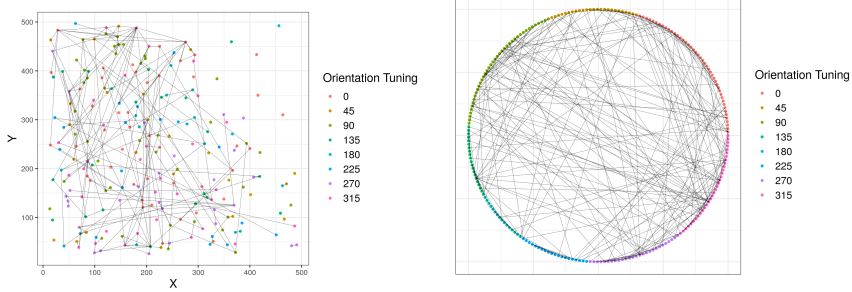
Model	Baseline			
	TPR	FDP		
Extreme (4)	0.690 (0.060)	0.303 (0.068)		
Extreme (6)	0.751 (0.062)	0.244 (0.063)		
Extreme (8)	<b>0.782</b> (0.067)	<b>0.205</b> (0.070)		
Gaussian Glasso	0.411 (0.068)	0.582 (0.071)		
Gaussian NS	0.395 (0.065)	0.604 (0.062)		
Quantile (0.5)	0.066 (0.022)	0.940 (0.017)		
Quantile (0.9)	0.506 (0.067)	0.494 (0.070)		
Quantile (0.99)	0.650 (0.072)	0.339 (0.079)		
Quantile (0.999)	0.524 (0.076)	0.475 (0.074)		
	$p = 300$		$p = 500$	
Model	TPR	FDP	TPR	FDP
	0.578 (0.070)	0.423 (0.068)	0.452 (0.073)	0.551 (0.070)
Extreme (6)	0.624 (0.074)	0.373 (0.077)	0.533 (0.078)	0.462 (0.072)
Extreme (8)	<b>0.697</b> (0.072)	<b>0.299</b> (0.071)	<b>0.591</b> (0.079)	<b>0.407</b> (0.079)
Gaussian Glasso	0.376 (0.062)	0.623 (0.063)	0.302 (0.065)	0.699 (0.068)
Gaussian NS	0.349 (0.061)	0.653 (0.064)	0.263 (0.059)	0.734 (0.062)
Quantile (0.5)	0.050 (0.015)	0.952 (0.018)	0.055 (0.018)	0.944 (0.016)
Quantile (0.9)	0.451 (0.065)	0.552 (0.062)	0.426 (0.061)	0.575 (0.064)
Quantile (0.99)	0.589 (0.072)	0.411 (0.074)	0.536 (0.076)	0.465 (0.076)
Quantile (0.999)	0.533 (0.071)	0.469 (0.075)	0.497 (0.077)	0.502 (0.078)
	$0.0005Hz$		$0.002Hz$	
Model	TPR	FDP	TPR	FDP
	0.804 (0.068)	0.198 (0.065)	0.463 (0.062)	0.539 (0.069)
Extreme (6)	0.832 (0.069)	0.170 (0.060)	0.547 (0.065)	0.464 (0.063)
Extreme (8)	<b>0.855</b> (0.074)	<b>0.147</b> (0.071)	<b>0.611</b> (0.071)	<b>0.392</b> (0.069)
Gaussian Glasso	0.399 (0.061)	0.599 (0.057)	0.444 (0.067)	0.551 (0.062)
Gaussian NS	0.383 (0.053)	0.620 (0.059)	0.426 (0.067)	0.568 (0.066)
Quantile (0.5)	0.051 (0.028)	0.947 (0.021)	0.087 (0.019)	0.914 (0.020)
Quantile (0.9)	0.602 (0.072)	0.390 (0.070)	0.351 (0.072)	0.653 (0.069)
Quantile (0.99)	0.725 (0.076)	0.279 (0.077)	0.439 (0.073)	0.559 (0.074)
Quantile (0.999)	0.594 (0.072)	0.408 (0.075)	0.433 (0.079)	0.571 (0.077)
	$\mu = 12$		$\mu = 16$	
Model	TPR	FDP	TPR	FDP
	0.411 (0.062)	0.586 (0.065)	0.476 (0.066)	0.524 (0.071)
Extreme (6)	0.452 (0.060)	0.549 (0.069)	0.527 (0.069)	0.485 (0.073)
Extreme (8)	<b>0.468</b> (0.068)	<b>0.539</b> (0.071)	<b>0.587</b> (0.064)	<b>0.412</b> (0.067)
Gaussian Glasso	0.322 (0.065)	0.671 (0.067)	0.368 (0.067)	0.641 (0.068)
Gaussian NS	0.311 (0.070)	0.684 (0.069)	0.344 (0.062)	0.658 (0.065)
Quantile (0.5)	0.045 (0.012)	0.944 (0.010)	0.052 (0.011)	0.952 (0.012)
Quantile (0.9)	0.323 (0.065)	0.682 (0.072)	0.437 (0.071)	0.565 (0.064)
Quantile (0.99)	0.318 (0.074)	0.584 (0.073)	0.479 (0.078)	0.521 (0.079)
Quantile (0.999)	0.278 (0.077)	0.726 (0.071)	0.415 (0.072)	0.582 (0.073)

The numerical results from the simulation study are shown in Table 2. As a whole, we see that the extreme graphical model does the best in terms of estimating the true graph structure of the balanced network. The true positive and false discovery rates for the extreme graphical model are notably better than any of the other competing models; only the quantile graphical model at the 99th percentile is close. Interestingly, the quantile graphical model at the 99.9th percentile actually performs worse than at the 99th percentile. This highlights that, for analyzing extreme values, the selection of quantile can have a large impact on the resulting graphical model estimate and that choosing the correct quantile is not simply a question of choosing as large of a quantile as computationally possible. We also note the median quantile graphical model performs particularly poorly in this set of simulations because it is more robust to rare extreme values relative to the Gaussian or extreme graphical model by design, meaning that it puts even less relative weight on the extreme values when performing parameter estimation. As expected, increasing the number of simulated neurons in the system decreases the accuracy of all methods. Also unsurprisingly, decreasing the average magnitudes of the simulated spikes decreases the performance of all methods with respect to finding the graph structure with respect to these observations. Interestingly, decreasing the number of spikes per neuron actually leads to better performance from all methods; this could be caused by a resulting decrease in the number of true edges of the graph as well as a smaller probability of finding a false positive match between a true extreme observation and a noise observation.

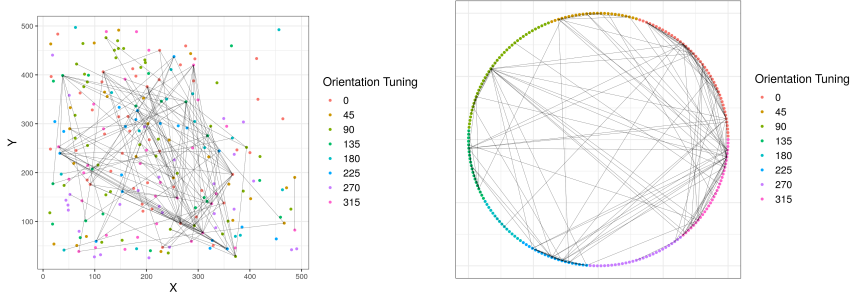
## 5 Functional Neuronal Connectivity Case Study

Lastly, we investigate the applicability of the extreme graphical model to estimating functional neuronal connectivity networks for real-world calcium imaging data. We use a data set originally from the Allen Brain Atlas (Lein et. al., 2007) which has fluorescence traces for 227 neurons in the visual cortex of the brain of a mouse at over 100000 time point observations; for this particular case study, we examine a subset of 18000 time points from this data set during a period of controlled drifting grating visual stimulus activity. We estimate a functional neuronal connectivity graph for a Gaussian graphical model and for the extreme graphical model with  $\nu = 8$ . For the Gaussian graphical model, we use the neighborhood selection approach for edge selection. Hyperparameter selection for  $\lambda$  is performed for both graphical models using stability selection.

In Figure 1, we show the functional neuronal connectivity estimates from both methods, with each graph estimate plotted with respect to the spatial locations of the neurons and as a circle graph. Here, we specifically compare the selected edges with respect to the orientation tunings of the pairs of neurons in the edge set. It is hypothesized in the neuroscience literature that neurons are tuned to fire when presented with particular stimuli, and that these neurons are more likely to



(a) Gaussian graphical model estimate, shown with real neuron locations (left) and as a circle graph (right).



(b) Extreme graphical model estimate, shown with real neuron locations (left) and as a circle graph (right).

Fig. 1: Comparison of the functional connectivity estimates from the Gaussian graphical model and the extreme graphical model. 60.1% of edges in the extreme graph estimate are between neurons with the same tuning, as opposed to 36.9% for the Gaussian graph estimate.

be connected functionally (Sakia and Miyashita, 1994). In the graph estimates, 60.1% of edges in the extreme graphical model are between neurons with the same tuning, as opposed to 36.9% for the Gaussian graphical model; this provides us with some evidence that the functional connectivity estimate from the extreme graphical model is more scientifically appropriate compared to that from the Gaussian graphical model. We also see from the circle graphs in Figure 1 that the functional connectivity estimate from the extreme graphical model exhibits much more of a small-world structure compared to that from the Gaussian graphical model.

We then compare the selected edges for the largest degree hub neurons in the estimated functional connectivity graphs from the extreme graphical model and from the Gaussian graphical model. In Figure 2, we show the fluorescence traces for each respective hub neuron and its neighbors plotted on top of one another. The fluorescence traces of the hub neuron of the Gaussian graphical model and its

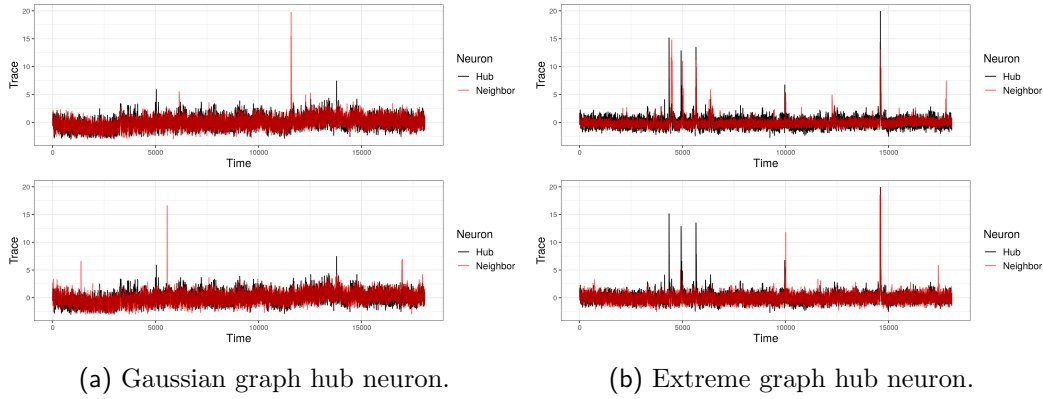


**Fig. 2:** Trace of different high degree hub neurons (black) vs. traces of selected edge neighbors (red) in functional connectivity estimates from the Gaussian and extreme graphical models.

neighbors, as seen in Figure 2a, display a similar baseline mean shift pattern across time, possibly caused by artifacts of the data collection methodology. However, there are clearly no relationships between the hub neuron and any of the selected neighbors with respect to any extreme value spikes in the fluorescence traces, and it does not appear that the selected hub neuron is particularly active at all during the recorded time period. On the other hand, the hub neuron of the extreme graphical model clearly fire simultaneously with its selected graph neighbors more than once during the experiment, as seen in Figure 2b. Thus, the edges from the extreme graphical model appear to be much more likely to be scientifically meaningful compared to those from the Gaussian graphical model.

We also show the differences in the edges selected for the same neuron in both graph estimates in Figure 3. The neuron we highlight here has several edge neighbors in the estimated networks for both the Gaussian and extreme graphical models, but the neighbors selected by each method are different. We can see from Figure 3a that the neighbors in the graph estimated by the Gaussian graphical model do not appear to share any similar spiking patterns with the highlighted neuron. On the other hand, as seen from Figure 3b, the edge neighbors as selected by the extreme graphical model for the exact same neuron seem to spike at the same time at one particular time point during the recording. From this example, the extreme graphical model seems to do a better job of finding neurons which share similar spiking patterns, as is the goal when estimating functional neuronal connectivity networks.

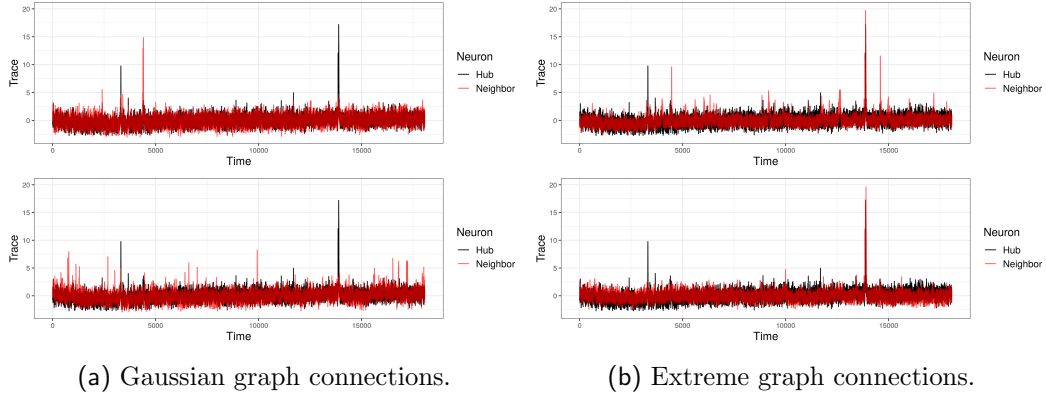


**Fig. 3:** Trace of single particular neuron (black) vs. trace of selected edge neighbors (red) in functional connectivity estimates from the Gaussian and extreme graphical models.

## 6 Discussion

In this paper, we have introduced the extreme graphical model for estimating networks for data in which the primary focus of the analysis is on finding the conditional dependency structure with respect to the extreme value observations. Our model is constructed by defining the node-wise conditional distribution of the graphical model as a generalized normal distribution with  $\nu > 2$ , which increases the relative weight of extreme values in the estimation process compared to the Gaussian graphical model. Our proposed extreme graphical model has several advantages over other methods currently used for this type of analysis; it does not require any data pre-processing to identify extreme values before model estimation in order to produce meaningful results, it is not highly dependent on any priori choices of hyperparameter, and it smoothly upweights the extreme value observations with respect to their magnitudes. Through simulation studies and a real-world example, we have shown the potential usefulness of the extreme graphical model to analyzing data with extreme value observations. Additionally, we showed the suitability of our model to neuroscientific applications, specifically toward estimating functional neuronal connectivity graphs for calcium imaging data. We also have demonstrated selection consistency for and the finite sample performance of the estimator of the edge set of the true graph.

There are several possible areas of research for the extreme graphical model that can be explored in future works. From a methodological standpoint, we have used ordinary bootstrapping sampling with our stability selection method in order to select the hyperparameter values for the individual node-wise regressions. However, this type of procedure may not be the most appropriate when the main focus of the analysis is on the rare extreme value observations, and there may be better schemes

that could be implemented for this part of the algorithm. Also, like with the Gaussian graphical model, there are many potential extensions to the extreme graphical model that could be developed to account for different experimental conditions or possible effects. For example, in neuroscience, common implementations of graphical model methods include latent variable adjustments to adjust for the potential impact of unmeasured brain neuron activity or stimuli and changepoint methods to create smoothly varying functional neuronal connectivity estimates under different experimental stimuli conditions.

We also note here that the extreme graphical model that we have developed is in this paper is based on an assumption of i.i.d observations. However, in many examples of data sets for which our model may be relevant, such as calcium imaging data, it is often assumed that the observed features follow some type of time series model (Pnevmatikakis et. al., 2016). While the extreme graphical model described in this work does not specifically handle autocorrelation effects, previous literature shows that it can still work with this type of data. Specifically, in (Basu and Michailidis, 2013), it is shown that Lasso-based sparse estimators, such as the one used for the extreme graphical model, are still model selection consistent though with the a larger theoretical sample complexity. Because the number of observed time points in data sets where rare extreme value observations are the focal point of analysis is often large relative to the number of features, we believe our method will work well even in the presence of autocorrelation effects. Nevertheless, a methodological extension for time series data could be a pertinent area of investigation for future work.

The extreme graphical model has the potential to be explored further on the application side as well. Within the realm of neuroscience, our model could be used to study neuronal functional connectivity networks for calcium imaging data on a much larger scope than the one considered in this paper, with possibly up to tens of thousands of *in vivo* simultaneously recorded neurons. These studies can help provide new insights into the how individual neurons in the brain are organized functionally on a large-scale basis. Another open neuroscience research topic for which our method could be applied is on the relationship between functional and structural connectivity in the brain. One particular interesting study could involve comparing how closely estimated functional connectivity network from both our model as well as others common techniques in the literature match the brain's physical structure, while also attempting to characterize how certain patterns in neuronal activity may create differences between the two. Additionally, while the main focus of the paper has involved relating our method to neuroscience experiments, there are several other fields in which the extreme graphical model could be utilized, including climatology, signal processing, and finance. In conclusion, our work has created a new single-step graphical model method which could provide a more accurate method for estimating scientifically meaningful networks for data in which the important information in the data involves the extreme value observations.

## A Proofs

### A.1 Proof of Theorem 1

Our derivation of the functional form of the joint distribution follows from Besag (1974), which showed that a valid multivariate joint distribution can be derived from a known conditional distribution via the equivalency

$$Q(\mathbf{x}) = \prod_{i=1}^p \frac{P(x_i|x_1, x_2, \dots, x_{i-1}, y_{i+1}, \dots, y_p)}{P(y_i|x_1, x_2, \dots, x_{i-1}, y_{i+1}, \dots, y_p)}$$

(Note that since the distribution is supported on the entirety of  $\mathbb{R}^p$ , the necessary assumption of a non-zero probability for all denominators is fulfilled.) We derive the exponential functional form of the joint distribution in Theorem 1 by defining

$$Q(\mathbf{x}) := \log(P(\mathbf{x})/P(\mathbf{0})),$$

which can be shown to be equivalent to

$$Q(\mathbf{x}) = \log \left( \prod_{i=1}^p \frac{P(x_i|x_1, x_2, \dots, x_{i-1}, y_{i+1} = 0, \dots, y_p = 0)}{P(y_i = 0|x_1, x_2, \dots, x_{i-1}, y_{i+1} = 0, \dots, y_p = 0)} \right).$$

We then replace  $Q(\mathbf{x})$  with the Hammersley-Clifford definition of the most general form of a graphical model joint distribution to get:

$$\sum_{1 \leq i \leq p} x_i G_i(x_i) + \sum_{1 \leq i \leq j \leq p} x_i x_j G_{ij}(x_i, x_j) + \dots = \log \left( \prod_{i=1}^p \frac{P(x_i|x_1, x_2, \dots, x_{i-1}, y_{i+1} = 0, \dots, y_p = 0)}{P(y_i = 0|x_1, x_2, \dots, x_{i-1}, y_{i+1} = 0, \dots, y_p = 0)} \right).$$

For our particular case, there will be interaction terms in the Hammersley-Clifford form of the distribution up to the  $\nu$ -th order. We can then find equivalencies between individual terms on the left and right hand sides of the above equation. Without loss of generality, we first operate on  $\mathbf{x}_p$ . Define:

$$\mathbf{x}_{i:0} := (x_1, \dots, x_{i-1}, 0, x_{i+1}, \dots, x_p).$$

By definition, we have

$$\frac{\exp(Q(\mathbf{x}))}{\exp(Q(\mathbf{x}_{p:0}))} = \exp(Q(\mathbf{x}) - Q(\mathbf{x}_{p:0})) = x_p \left( G_p(x_p) + \sum_{1 \leq i \leq p-1} x_i G_{ip}(x_i, x_p) \right)$$

and

$$\frac{\exp(Q(\mathbf{x}))}{\exp(Q(\mathbf{x}_{p:0}))} = \frac{P(\mathbf{x})}{P(\mathbf{x}_{p:0})} = \frac{P(x_p|x_1, x_2, \dots, x_{p-1})}{P(x_p = 0|x_1, x_2, \dots, x_{p-1})}.$$

The two above equations allows us to isolate only those terms which are functions of  $x_p$ . The latter equation also gives us the first term of the product  $\prod_{i=1}^p \frac{P(x_i|x_1, x_2, \dots, x_{i-1}, y_{i+1}=0, \dots, y_p=0)}{P(y_i=0|x_1, x_2, \dots, x_{i-1}, y_{i+1}=0, \dots, y_p=0)}$ . Specifically we get:

$$\begin{aligned} x_p \left( G_p(x_p) + \sum_{1 \leq i \leq p-1} x_i G_{ip}(x_i, x_p) + \dots \right) &= \frac{P(x_p|x_1, x_2, \dots, x_{p-1})}{P(x_p=0|x_1, x_2, \dots, x_{p-1})} \\ &= \exp \left( -(x_p - \sum_{i \leq p-1} \theta_{ip} x_i)^\nu + (\sum_{i \leq p-1} \theta_{ip} x_i)^\nu \right) \end{aligned}$$

Using arithmetic to expand the right hand side of the above equation, we can find each individual  $G$  function:

$$\begin{aligned} G_p(x_p) &= -x_p^{\nu-1}, \\ G_{ip}(x_i, x_p) &= -\theta_{ip} ((x_p - \theta_{ip} x_i)^{\nu-2} - (\theta_{ip} x_i)^{\nu-1}), \\ G_{ijp}(x_i, x_j, x_p) &= -\theta_{ip} \theta_{jp} ((x_p - \theta_{ip} x_i - \theta_{jp} x_j)^{\nu-3} - (\theta_{ip} x_i - \theta_{jp} x_j)^{\nu-2}), \end{aligned}$$

and so on, up to the  $\nu$ -th order  $G$  function. One particular thing to note is that, if  $\theta_{ip} = 0$ , then all  $G$  functions involving  $x_i$  and  $x_p$  will be equal to 0, meaning that this is a valid form for the joint probability distribution by the Hammersley-Clifford theorem. We can then operate recursively to get the  $G$  functions for all  $r \in 1, 2, \dots, p$ . For example, for  $x_{p-1}$ , we get:

$$\begin{aligned} x_{p-1} \left( G_{p-1}(x_{p-1}) + \sum_{1 \leq i \leq p-2} x_i G_{i(p-1)}(x_i, x_{p-1}) + \dots \right) &= \frac{P(x_{p-1}|x_1, x_2, \dots, x_{p-2}, x_p=0)}{P(x_{p-1}=0|x_1, x_2, \dots, x_{p-2}, x_p=0)} \\ &= \exp \left( -(x_{p-1} - \sum_{i \leq p-2} \theta_{ip} x_i)^\nu + (\sum_{i \leq p-2} \theta_{ip} x_i)^\nu \right) \end{aligned}$$

Putting all terms together for all variables gives us following functional form for the joint distribution:

$$\begin{aligned} Q(\mathbf{x}) &= \log \left( \prod_{i=1}^p \frac{P(x_i|x_1, x_2, \dots, x_{i-1}, y_{i+1}=0, \dots, y_p=0)}{P(y_i=0|x_1, x_2, \dots, x_{i-1}, y_{i+1}=0, \dots, y_p=0)} \right) \\ &= \sum_{i=1}^p \left( -(\theta_{ii} x_i - \sum_{j < i} \theta_{ij} x_j)^\nu + (\sum_{j < i} \theta_{ij} x_j)^\nu \right) \\ f(\mathbf{x}) &\propto \exp(Q(\mathbf{x})) \\ &\propto \exp \left( \sum_{i=1}^p \left( -(\theta_{ii} x_i - \sum_{j < i} \theta_{ij} x_j)^\nu + (\sum_{j < i} \theta_{ij} x_j)^\nu \right) \right). \end{aligned}$$

Adding the log normalizing constant to the distribution gives us:

$$f(\mathbf{x}) = \exp \left( \sum_{i=1}^p \left( -(\theta_{ii}x_i - \sum_{j < i} \theta_{ij}x_j)^\nu + (\sum_{j < i} \theta_{ij}x_j)^\nu \right) - A(\boldsymbol{\Theta}) \right).$$

□

## A.2 Proof of Theorem 2

We first discuss the relationship between  $\boldsymbol{\Theta}$  and the covariance of the distribution. Let  $\boldsymbol{\Sigma}$  be the covariance matrix of the extreme graphical model distribution. By the definition of the node-wise conditional distributions,  $\boldsymbol{\Theta}$  contains the partial correlations between all pairs of variables of the multivariate distribution. We can then combine the results from for the relationship between the partial correlation and precision matrices Lauritzen (1996) with the results from for the moments of univariate Subbotin distribution Nadarajah (2005), in order to find the relationship between  $\boldsymbol{\Sigma}$  and  $\boldsymbol{\Theta}$ :

$$\boldsymbol{\Sigma}_{ij}^{-1} = \begin{cases} \left( \frac{\Gamma(1/\nu)}{\Gamma(3/\nu)} \right) \theta_{ii} & i = j \\ -\left( \frac{\Gamma(1/\nu)}{\Gamma(3/\nu)} \right) \theta_{ij} & i \neq j \end{cases}.$$

Therefore, because the empirical  $\boldsymbol{\Sigma}$  must be positive definite by definition for any data set, the empirical  $\boldsymbol{\Theta}$  must be positive definite for any data set as well.

We now show that the condition in Theorem 2 is a necessary and sufficient condition for normalizability. Our proof requires the following lemma:

**Lemma 1.** Define

$$Q_{i,\nu}(x_i) = \left( -(\theta_{ii}x_i - \sum_{j < i} \theta_{ij}x_j)^\nu + (\sum_{j < i} \theta_{ij}x_j)^\nu \right)$$

where  $\nu$  is an even integer greater than 2. Then, for all  $i \in \{1, 2, \dots, p\}$ ,

1.  $\text{sign}(Q_{i,2}(x_i)) = \text{sign}(Q_{i,\nu}(x_i))$ .
2.  $\lim_{x_i \rightarrow \pm\infty} \frac{Q_{i,2}(x_i)}{Q_{i,\nu}(x_i)} = 0$ .

To prove the first part of Lemma 1, we exhaustively examine all possibilities for  $\text{sign}(Q_{i,2}(x_i))$ . We first note that

$$Q_{i,\nu}(x_i) = \left( -(\theta_{ii}x_i - \sum_{j < i} \theta_{ij}x_j)^\nu + (\sum_{j < i} \theta_{ij}x_j)^\nu \right)$$

$$= \left( -((\theta_{ii}x_i - \sum_{j < i} \theta_{ij}x_j)^2)^{\nu/2} + ((\sum_{j < i} \theta_{ij}x_j)^2)^{\nu/2} \right).$$

If  $\text{sign}(Q_{i,2}(x_i)) = +1$ , then

$$(\theta_{ii}x_i - \sum_{j < i} \theta_{ij}x_j)^2 < (\sum_{j < i} \theta_{ij}x_j)^2.$$

It then follows that

$$((\theta_{ii}x_i - \sum_{j < i} \theta_{ij}x_j)^2)^{\nu/2} < ((\sum_{j < i} \theta_{ij}x_j)^2)^{\nu/2}$$

since the transformation operator in this case is monotonically increasing. Thus, in this case, we have that  $\text{sign}(Q_{i,\nu}(x_i)) = +1$  as well. Similarly, if  $\text{sign}(Q_{i,2}(x_i)) = -1$ , then we have

$$(\theta_{ii}x_i - \sum_{j < i} \theta_{ij}x_j)^2 > (\sum_{j < i} \theta_{ij}x_j)^2.$$

Using the same argument as above, this implies that

$$((\theta_{ii}x_i - \sum_{j < i} \theta_{ij}x_j)^2)^{\nu/2} > ((\sum_{j < i} \theta_{ij}x_j)^2)^{\nu/2}.$$

Therefore, in this scenario,  $\text{sign}(Q_{i,\nu}(x_i)) = -1$  as well. The second part of Lemma 1 can be shown simply by direct comparison:

$$\begin{aligned} & \lim_{x_i \rightarrow \pm\infty} \frac{Q_{i,2}(x_i)}{Q_{i,\nu}(x_i)} \\ &= \lim_{x_i \rightarrow \pm\infty} \frac{1}{-(\theta_{ii}x_i - \sum_{j < i} \theta_{ij}x_j)^{\nu-2}} + o(1) \\ &= 0 \end{aligned}$$

We now use the statement of Lemma 1 to show necessity and sufficiency for the condition of Theorem 2. To do this, we utilize the known normalizability condition of the extreme graphical model for  $\nu = 2$ , i.e. when the extreme graphical model is equivalent to a multivariate Gaussian distribution. Define

$$Q_\nu(\mathbf{x}) = \sum_{i=1}^p \left( -(\theta_{ii}x_i - \sum_{j < i} \theta_{ij}x_j)^\nu + (\sum_{j < i} \theta_{ij}x_j)^\nu \right).$$

If  $\Theta$  is positive definite, then we know from previous results on the multivariate Gaussian that  $\forall i \in \{1, 2, \dots, p\}$ ,

$$\lim_{x_i \rightarrow \pm\infty} \exp(Q_{i,2}(\mathbf{x})) = 0$$

and therefore

$$\int_{-\infty}^{\infty} \int_{-\infty}^{\infty} \int_{-\infty}^{\infty} \dots \exp(Q_2(\mathbf{x})) dx_1 dx_2 dx_3 \dots$$

is finite. From Lemma 1, it can be shown that for any even integer  $\nu$  greater than 2:

$$\forall i \in \{1, 2, \dots, p\} : \lim_{x_i \rightarrow \infty} \frac{\exp(Q_{i,\nu}(\mathbf{x}))}{\exp(Q_{i,2}(\mathbf{x}))} = 0.$$

Thus, we have that  $\forall i \in \{1, 2, \dots, p\}$ ,

$$\lim_{x_i \rightarrow \pm\infty} \exp(Q_{i,\nu}(\mathbf{x})) = 0$$

and therefore

$$\int_{-\infty}^{\infty} \int_{-\infty}^{\infty} \int_{-\infty}^{\infty} \dots \exp(Q_{\nu}(\mathbf{x})) dx_1 dx_2 dx_3 \dots$$

will be finite as well. Thus, the condition of Theorem 2 is a sufficient condition for normalizability. On the other hand, if  $\Theta$  is not positive definite, then  $\exists i \in \{1, 2, \dots, p\}$ ,

$$\lim_{x_i \rightarrow \pm\infty} \exp(Q_{i,2}(\mathbf{x})) = \infty.$$

Therefore,

$$\int_{-\infty}^{\infty} \int_{-\infty}^{\infty} \int_{-\infty}^{\infty} \dots \exp(Q_2(\mathbf{x})) dx_1 dx_2 dx_3 \dots$$

will be divergent. From Lemma 1, we have that for any even integer  $\nu$  greater than 2:

$$\forall i \in \{1, 2, \dots, p\} : \lim_{x_i \rightarrow \infty} \frac{\exp(Q_{i,2}(\mathbf{x}))}{\exp(Q_{i,\nu}(\mathbf{x}))} = \infty.$$

Thus, by the limit comparison test,  $\exists i \in \{1, 2, \dots, p\}$  such that

$$\lim_{x_i \rightarrow \pm\infty} Q_{i,\nu}(x_i) < 0$$

and

$$\int_{-\infty}^{\infty} \int_{-\infty}^{\infty} \int_{-\infty}^{\infty} \dots \exp(-Q_{\nu}(\mathbf{x})) dx_1 dx_2 dx_3 \dots$$

will be divergent as well, meaning that  $A(\Theta)$  will not exist. Thus, the condition of Theorem 2 is a necessary condition for normalizability.  $\square$

### A.3 Proof of Theorem 3

For this proof, we apply previous theoretical results for variable selection consistency for the Extreme Lasso regression which we utilize as the node-wise conditional regression problem for the extreme graphical model. We first provide the statement for the finite sample convergence rate and variable selection consistency of the Extreme Lasso problem; this corresponds to Theorem 3.4 in (Chang, Wang, and Allen, 2020). The full proof can be found in the aforementioned paper.

**Lemma 2 (Neighborhood Selection Consistency).** Consider the Extreme Lasso program for the node-wise conditional regression problem. Assume that conditions 1 and 2 from section 3 hold. Consider the family of regularization parameters  $\lambda = \frac{4\kappa_{IC}}{\tau} \gamma \sqrt{\frac{\log p}{n}} \left[ 2\sqrt{\frac{2}{\gamma}} + \sqrt{\frac{\log p}{n}} \right]$ , where  $\kappa_{IC}$  is the compatibility constant defined in Lee (2015). Then the following properties holds with probability greater than  $1 - c_1 \exp(-c_2^* \log p)$ :

- (i) The Lasso has a unique solution with support contained within  $S_i$  i.e.,  $\hat{S}_i \subset S_i$ .
- (ii) If condition 3 holds, the lasso estimator is also sign consistent:  $\text{sign}(\hat{\theta}_{ij}) = \text{sign}(\theta_{ij})$ .

The full proof can be found in the aforementioned paper. From Lemma 2, we can use a simple union bound on all node neighborhoods to derive the probability of model selection consistency for the full graph. If variable selection consistency holds for a single neighborhood with probability

$$1 - c_1 \exp(-c_2^* \log p),$$

then it does not hold with probability

$$c_1 \exp(-c_2^* \log p).$$

Thus, the probability of any neighborhood not holding will be bounded above by

$$pc_1 \exp(-c_2^* \log p).$$

Therefore, the probability of achieving consistent model selection for the entire graph will be bounded below by

$$1 - c_1 \exp(-c_2^* \log p + \log p).$$

We can then define  $c_2 = c_2^* - 1$  to get

$$1 - c_1 \exp(-c_2 \log p).$$

□

## B Simulation Study: Data Driven Tuning

### B.1 Extreme Graphical Model Distribution

Table 3 shows the results from the joint extreme graphical model distribution simulations for data-driven model selection via stability selection. Here, all methods applied appear to overselect the number of edges in the graph. We see similar patterns in terms of changes in variable selection accuracy for adjusting the simulation parameters that we see in the oracle tuning example. However, here we see that,

in certain cases, the extreme graphical model method at  $\nu = 8$  does not always have the best true positive rate or false discovery proportion, even when it is the true value of  $\nu$  from the simulation. However, even when these situations arise, the extreme graphical model at a smaller value of  $\nu$  still outperforms the Gaussian or quantile graphical models.

Tab. 3: Average TPR, FDP. (std. devs) for multivariate extreme graphical model distribution simulations with stability selection, averaged over 5 replicates. Best performing methods are boldfaced.

Model	Baseline			
	TPR	FDP	TPR	FDP
Extreme (4)	0.783 (0.072)	0.267 (0.070)		
Extreme (6)	0.826 (0.075)	0.269 (0.064)		
Extreme (8)	<b>0.855</b> (0.069)	<b>0.257</b> (0.072)		
Gaussian Glasso	0.761 (0.072)	0.353 (0.069)		
Gaussian NS	0.744 (0.068)	0.369 (0.062)		
Quantile (0.5)	0.624 (0.065)	0.355 (0.069)		
Quantile (0.9)	0.258 (0.063)	0.730 (0.068)		
	<i>n</i> = 1000		<i>n</i> = 4000	
Model	TPR	FDP	TPR	FDP
	0.529 (0.079)	0.549 (0.066)	0.842 (0.065)	0.229 (0.064)
Extreme (6)	0.555 (0.072)	0.542 (0.061)	0.854 (0.073)	<b>0.226</b> (0.065)
Extreme (8)	<b>0.623</b> (0.075)	<b>0.501</b> (0.067)	<b>0.878</b> (0.071)	0.235 (0.067)
Gaussian Glasso	0.484 (0.072)	0.571 (0.069)	0.852 (0.062)	0.270 (0.069)
Gaussian NS	0.491 (0.077)	0.554 (0.082)	0.823 (0.062)	0.266 (0.065)
Quantile (0.5)	0.466 (0.068)	0.582 (0.080)	0.817 (0.077)	0.250 (0.071)
Quantile (0.9)	0.223 (0.067)	0.771 (0.062)	0.301 (0.067)	0.697 (0.064)
	<i>p</i> = 300		<i>p</i> = 1000	
Model	TPR	FDP	TPR	FDP
	0.636 (0.079)	0.343 (0.074)	0.478 (0.077)	0.586 (0.065)
Extreme (6)	0.697 (0.075)	0.279 (0.072)	<b>0.545</b> (0.071)	0.527 (0.063)
Extreme (8)	<b>0.708</b> (0.068)	<b>0.366</b> (0.065)	0.536 (0.071)	<b>0.517</b> (0.070)
Gaussian Glasso	0.627 (0.073)	0.506 (0.074)	0.439 (0.077)	0.692 (0.078)
Gaussian NS	0.651 (0.068)	0.463 (0.071)	0.457 (0.073)	0.629 (0.072)
Quantile (0.5)	0.551 (0.065)	0.539 (0.069)	0.424 (0.072)	0.677 (0.070)
Quantile (0.9)	0.224 (0.055)	0.780 (0.060)	0.109 (0.052)	0.923 (0.054)
	$\nu$ = 4		$\nu$ = 6	
Model	TPR	FDP	TPR	FDP
	0.906 (0.055)	<b>0.197</b> (0.059)	0.815 (0.061)	0.270 (0.062)
Extreme (6)	0.859 (0.061)	0.244 (0.058)	<b>0.876</b> (0.057)	<b>0.147</b> (0.056)
Extreme (8)	0.757 (0.061)	0.271 (0.060)	0.764 (0.067)	0.338 (0.063)
Gaussian Glasso	0.855 (0.072)	0.197 (0.067)	0.811 (0.065)	0.284 (0.067)
Gaussian NS	0.836 (0.068)	0.198 (0.065)	0.824 (0.062)	0.279 (0.063)
Quantile (0.5)	0.620 (0.076)	0.416 (0.061)	0.617 (0.067)	0.409 (0.077)
Quantile (0.9)	0.287 (0.062)	0.721 (0.068)	0.232 (0.064)	0.776 (0.057)
	Chain		Erdos-Renyi	
Model	TPR	FDP	TPR	FDP
	0.652 (0.064)	0.357 (0.078)	<b>0.623</b> (0.077)	<b>0.426</b> (0.073)
Extreme (6)	0.667 (0.072)	0.355 (0.077)	0.601 (0.070)	0.454 (0.078)
Extreme (8)	<b>0.695</b> (0.075)	<b>0.312</b> (0.077)	0.608 (0.078)	0.450 (0.071)
Gaussian Glasso	0.606 (0.071)	0.486 (0.069)	0.571 (0.073)	0.456 (0.074)
Gaussian NS	0.587 (0.079)	0.480 (0.078)	0.574 (0.061)	0.457 (0.077)
Quantile (0.5)	0.550 (0.073)	0.455 (0.071)	0.534 (0.075)	0.475 (0.069)
Quantile (0.9)	0.182 (0.051)	0.790 (0.060)	0.191 (0.054)	0.788 (0.058)

## B.2 Artificial Neuronal Network

Table 4 shows the results from the balanced neuronal network simulations for data-driven model selection via stability selection. We see here that all methods tend to underselect the total number of edges in the simulated functional connectivity graph. This is to be expected, since the data are convoluted with uncorrelated white noise. In all cases, the extreme graphical model always has the best true positive rate and false discovery proportions, although the optimal value of  $\nu$  changes depending on the simulation scenario. In particular, a smaller value of  $\nu$  appears to perform better for higher spiking rates and for smaller spikes.

Tab. 4: Average TPR, FDP. (std. devs) for balanced neuronal network simulations with stability selection, averaged over 5 replicates. Best performing methods are boldfaced.

Model	Baseline			
	TPR	FDP		
Extreme (4)	0.614 (0.075)	0.316 (0.074)		
Extreme (6)	0.695 (0.071)	0.277 (0.072)		
Extreme (8)	<b>0.707</b> (0.067)	<b>0.205</b> (0.071)		
Gaussian Glasso	0.231 (0.069)	0.409 (0.091)		
Gaussian NS	0.194 (0.061)	0.421 (0.098)		
Quantile (0.5)	0.035 (0.015)	0.611 (0.055)		
Quantile (0.9)	0.482 (0.072)	0.454 (0.071)		
Quantile (0.99)	0.548 (0.077)	0.433 (0.068)		
Quantile (0.999)	0.474 (0.083)	0.451 (0.067)		
	$p = 300$		$p = 500$	
Model	TPR	FDP	TPR	FDP
	0.556 (0.069)	0.325 (0.081)	0.423 (0.075)	0.441 (0.084)
Extreme (6)	0.581 (0.071)	0.272 (0.076)	0.506 (0.078)	0.296 (0.081)
Extreme (8)	<b>0.652</b> (0.068)	<b>0.236</b> (0.089)	<b>0.547</b> (0.067)	<b>0.327</b> (0.083)
Gaussian Glasso	0.207 (0.059)	0.527 (0.102)	0.195 (0.047)	0.532 (0.101)
Gaussian NS	0.172 (0.055)	0.471 (0.088)	0.177 (0.061)	0.484 (0.095)
Quantile (0.5)	0.020 (0.015)	0.606 (0.051)	0.022 (0.012)	0.625 (0.050)
Quantile (0.9)	0.442 (0.071)	0.477 (0.082)	0.407 (0.065)	0.487 (0.083)
Quantile (0.99)	0.478 (0.067)	0.438 (0.063)	0.433 (0.073)	0.462 (0.080)
Quantile (0.999)	0.455 (0.063)	0.421 (0.078)	0.396 (0.076)	0.518 (0.082)
	$0.0005\text{Hz}$		$0.002\text{Hz}$	
Model	TPR	FDP	TPR	FDP
	0.622 (0.072)	0.309 (0.067)	0.591 (0.061)	0.312 (0.075)
Extreme (6)	0.703 (0.064)	0.275 (0.077)	<b>0.673</b> (0.063)	<b>0.277</b> (0.072)
Extreme (8)	<b>0.745</b> (0.073)	<b>0.251</b> (0.071)	0.654 (0.080)	0.310 (0.082)
Gaussian Glasso	0.217 (0.068)	0.454 (0.089)	0.265 (0.057)	0.484 (0.085)
Gaussian NS	0.218 (0.061)	0.437 (0.078)	0.244 (0.055)	0.403 (0.088)
Quantile (0.5)	0.028 (0.011)	0.592 (0.041)	0.043 (0.011)	0.620 (0.062)
Quantile (0.9)	0.527 (0.079)	0.361 (0.079)	0.377 (0.062)	0.524 (0.082)
Quantile (0.99)	0.627 (0.078)	0.322 (0.086)	0.413 (0.077)	0.496 (0.089)
Quantile (0.999)	0.599 (0.088)	0.362 (0.089)	0.374 (0.072)	0.509 (0.083)
	$\mu = 12$		$\mu = 16$	
Model	TPR	FDP	TPR	FDP
	0.352 (0.064)	0.510 (0.074)	0.427 (0.076)	0.478 (0.082)
Extreme (6)	<b>0.391</b> (0.071)	<b>0.451</b> (0.076)	0.442 (0.071)	0.463 (0.083)
Extreme (8)	0.386 (0.070)	0.462 (0.083)	<b>0.517</b> (0.064)	<b>0.386</b> (0.078)
Gaussian Glasso	0.132 (0.069)	0.616 (0.091)	0.209 (0.069)	0.653 (0.093)
Gaussian NS	0.085 (0.034)	0.735 (0.076)	0.133 (0.041)	0.654 (0.107)
Quantile (0.5)	0.011 (0.010)	0.628 (0.065)	0.015 (0.012)	0.661 (0.073)
Quantile (0.9)	0.282 (0.063)	0.587 (0.082)	0.359 (0.077)	0.532 (0.091)
Quantile (0.99)	0.298 (0.066)	0.543 (0.087)	0.412 (0.077)	0.509 (0.076)
Quantile (0.999)	0.227 (0.078)	0.659 (0.099)	0.357 (0.083)	0.532 (0.087)

## Acknowledgements

The authors acknowledge support from NSF DMS-1554821, NSF NeuroNex-1707400, and NIH 1R01GM140468.

## References

Akil, A.E., Rosenbaum, R. and Josić, K. (2020). Synaptic Plasticity in Correlated Balanced Networks. *arXiv preprint arXiv:2004.12453*.

Ali, A., Kolter, J.Z. and Tibshirani, R.J. (2016). The multiple quantile graphical model. *arXiv preprint arXiv:1607.00515*

Allen, G.I. and Liu, Z. (2013). A local poisson graphical model for inferring networks from sequencing data. *IEEE transactions on nanobioscience* **12**(3), 189-198.

Basu, S. and Michailidis, G. (2013). Regularized estimation in sparse high-dimensional time series models. *The Annals of Statistics* **43**(4), 1535-1567.

Besag, J. (1974). Spatial interaction and the statistical analysis of lattice systems. *Journal of the Royal Statistical Society: Series B (Methodological)* **36**(2), 192-225.

Biswal, B., Zerrin Yetkin, F., Haughton, V. M., and Hyde, J. S. (1996). Functional connectivity in the motor cortex of resting human brain using echo-planar MRI. *Magnetic Resonance in Medicine* **34**(4), 537-541.

Buishand, T. A. (1989). Statistics of extremes in climatology. *Statistica Neerlandica* **1**, 1172-1188.

Chang, A., Yao, T. and Allen, G.I. (2019). Graphical models and dynamic latent factors for modeling functional brain connectivity. *2019 IEEE Data Science Workshop (DSW)*, 57-63.

Chang, A., Wang, M. and Allen, G.I. (2020). Sparse Regression for Extreme Values. *arXiv preprint arXiv:2007.04441*.

Goodman, I.R. and Kotz, S. (1973). Multivariate theta-generalized normal distributions. *Journal of Multivariate Analysis* **3**(2), 204-219.

Hammersley, J.M. and Clifford, P. (1971). Markov fields on finite graphs and lattices. *Unpublished manuscript*, 46.

Lauritzen, S.L. (1996). Graphical models (Vol. 17). Clarendon Press.

Lee, J.D. and Sun, Y. and Taylor, J.E. (2015). On model selection consistency of regularized M-estimators. *Electronic Journal of Statistics* **9**(1), 608-642.

Lein, E.S. and Hawrylycz, M.J. and Ao, N. and Ayres, M. and Bensinger, A. and Bernard, A. and Boe, A.F. and Boguski, M.S. and Brockway, K.S. and Byrnes, E.J. and Chen, L. (2007). Genome-wide atlas of gene expression in the adult mouse brain. *Nature* **445**(7124), 168-176.

Liu, H. and Roeder, K. and Wasserman, L. (2010). Stability approach to regularization selection (stars) for high dimensional graphical models. *Advances in neural information processing systems* **24**(2), 1432-1440.

Meinshausen, N. and Bühlmann, P. (2006). High-dimensional graphs and variable selection with the lasso. *Annals of statistics* **34**(3), 1436-1462.

Meinshausen, N. and Bühlmann, P. (2010). Stability selection. *Journal of the Royal Statistical Society: Series B (Statistical Methodology)* **72**(4), 417-473.

Money, A.H. and Affleck-Graves, J.F. and Hart, M.L. and Barr, G.D.I. (1982). The linear regression model: Lp norm estimation and the choice of p. *Communications in Statistics-Simulation and Computation* **11**(1), 89-109.

Nadarajah, S. (2005). A generalized normal distribution. *Journal of Applied statistics* **32**(7), 685-694.

Pnevmatikakis, E.A., Soudry, D., Gao, Y., Machado, T.A., Merel, J., Pfau, D., Reardon, T., Mu, Y., Lacefield, C., Yang, W. and Ahrens, M. (2016). Simultaneous denoising, deconvolution, and demixing of calcium imaging data. *Neuron* **89**(2), 285-299.

Ravikumar, P., Wainwright, M.J. and Lafferty, J.D. (2010). High-dimensional Ising model selection using l1-regularized logistic regression. *The Annals of Statistics* **38**(3), 1287-1319.

Rocco, M. (2014). Extreme value theory in finance: A survey. *Journal of Economic Surveys* **28**(1), 82-108.

Rossant, C., Kadir, S.N., Goodman, D.F., Schulman, J., Hunter, M.L., Saleem, A.B., Grosmark, A., Belluscio, M., Denfield, G.H., Ecker, A.S. and Tolias, A.S. (2016). Spike sorting for large, dense electrode arrays. *PLoS Comput Biol* **11**(3), e1004083.

Sakia, K. and Miyashita, Y. (1994). Neuronal tuning to learned complex forms in vision. *Neuroreport* **5**, 829-832.

Talih, M. and Hengartner, N. (2005). Structural learning with time-varying components: tracking the cross-section of financial time series. *Journal of the Royal Statistical Society: Series B (Statistical Methodology)* **67**(3), 321-341.

Verdoolaege, G. and Scheunders, P. (2012). On the geometry of multivariate generalized Gaussian models. *Journal of mathematical imaging and vision* **43**(3), 180-193.

Wang, T., Ren, Z., Ding, Y., Fang, Z., Sun, Z., MacDonald, M.L., Sweet, R.A., Wang, J. and Chen, W. (2016). FastGGM: an efficient algorithm for the inference of gaussian graphical model in biological networks. *PLoS computational biology* **12**(2), e1004755.

Yang, E., Ravikumar, P., Allen, G.I. and Liu, Z. (2012). Graphical models via generalized linear models. *NeurIPS* **25**, 1367-1375.

Yang, E., Ravikumar, P., Allen, G.I. and Liu, Z. (2015). Graphical models via univariate exponential family distributions. *The Journal of Machine Learning Research* **16**(1), 3813-3847.

Yatsenko, D., Josić, K., Ecker, A.S., Froudarakis, E., Cotton, R.J. and Tolias, A.S., (2015). Improved estimation and interpretation of correlations in neural circuits. *PLoS computational biology* **11**(3), e1004083.